Self-Epitaxial Hetero-Nanolayers and Surface Atom Reconstruction in Electrocatalytic Nickel Phosphides

Xian-Kui Wei,*,† Dehua Xiong,‡,§ Lifeng Liu,‡ and Rafal E. Dunin-Borkowski†

†Ernst Ruska-Centre for Microscopy and Spectroscopy with Electrons, Forschungszentrum Jülich GmbH, Jülich 52428, Germany

‡International Iberian Nanotechnology Laboratory (INL), Braga 4715-330, Portugal

§State Key Laboratory of Silicate Materials for Architectures, Wuhan University of Technology, Wuhan 430070, China

KEYWORDS: nickel phosphide, surface reconstruction, transmission electron microscopy, core-shell, water splitting, electron-beam bombardment

*Correspondence author E-mail: x.wei@fz-juelich.de (X.K.W.)

ABSTRACT:

Surface atomic, compositional and electronic structures play decisive roles in governing performance of the catalysts during electrochemical reactions. Nevertheless, for efficient and cheap transition-metal phosphides used for water splitting, such atomic-scale structural information is largely missing. Despite much effort being made so far, there is still a long way to go for establishing a precise structure-activity relationship. Here, in combination with electron-beam bombardment and compositional analysis, our atomic-scale transmission electron microscopy study on Ni_5P_4 nanosheets, with a preferential (001) orientation, directly reveals coverage of a self-epitaxial Ni_2P nanolayer on the phosphide surface. Apart from presence of nickel vacancies in the Ni_5P_4 phase, our quantum-mechanical image simulations also suggest the existence of an additional NiP_x ($0 < x < 0.5$) nanolayer, characteristic of complex surface atom reconstruction, on the outermost surface of the phosphides. The surface chemical gradient and the core-shell scenario, probably responsible for the passivated catalytic activity, unveil a novel insight to understand the catalytic performance of transition-metal catalysts used for electrochemical energy conversion.

INTRODUCTION

Sustainable production of chemical fuels through electrochemical reactions provides a promising solution for renewable energy storage and usage. Given the scarcity of ideal catalysts, usually precious metals, searching for highly efficient, active and cheap transition-metal catalysts such as carbides, phosphides and sulfides becomes one of the urgent tasks. [1-2] In recent years, transition-metal phosphides[3] such as Ni_2P, CoP, FeP and MoP have been reported to possess exceptional activity, efficiency and stability in water splitting,[4-12] hydrodesulfurization[13] and CO_2 reduction.[14] Compared with the rapidly-developed performance research, nevertheless, atomic-scale structural investigation in experiments is severely delayed or even overlooked.[15-16] Despite tremendous efforts from many pioneering works,[17-19] a long way is still ahead towards realizing rational design of robust catalysts.

Unveiling the surface atomic structure plays a key role in understanding the catalytic pathways for energy conversion.[20-21] Taking the two-dimensional (2D) MoS_2 as an example, its basal plane engineered by surface defects was found to be highly active for hydrogen evolution reaction (HER). Associated with transmission electron microscopy (TEM) characterization, it is shown that the superior activity is attributed to strained S-vacancies with tunability of the catalytic sites.[22-23] Besides deliberate exposure of the active sites,[24] proper surface sulfur doping on Ni_5P_4 and MoP[25-28] also show obvious improvement in performance of the catalysts. However, different from the typical 2D materials, these transition-metal catalysts are usually 3D in morphology. Although at nanometer scale, determining their 3D atomic structure, e.g., atomic arrangement and species on the surfaces, is very challenging. Therefore, our current understanding on the catalytic mechanism replies more on the theoretical models.[17-19, 29-30]

With respect to the Ni_2P phase,[7, 9] a general argument drawn from theoretical[18] and experimental[10, 31-32] studies shows that the Ni_5P_4 phase possesses a superior catalytic activity for hydrogen production. Nevertheless, except results from Laursen *et al*.,[7, 10] there has been no other results reporting that the performance of the Ni_5P_4 phase is comparable to that of Pt catalyst. Associated with a survey of the Ni/P composition ratio, the catalytic performance of pure Ni_5P_4 phase relating to the precursors, synthesis methods and electrolytes are summarized in **Table 1**. It is seen that phosphorus tends to be enriched in the Ni_5P_4 microparticles that possess the best HER activity, which is supported by density functional theory (DFT) calculations[17-18]. While for other sample forms, e.g., film, nanocrystals and nanosheets, the Ni tends to be enriched on the Ni_5P_4 phase with the inferior activity.

In this work, to better configure the structure-activity relationship, we investigate the atomic structures of (001)-oriented Ni_5P_4 nanosheets, synthesized by vapor phosphorization to Ni foam,[5] by using atomic-resolution scanning/transmission electron microscopy (S/TEM). Our study reveals that the surface structures of the Ni_5P_4 nanosheets are much more complex than our traditional cognition. Being consistent with the compositional analysis, our electron-beam irradiation experiments directly reveal a self-epitaxial Ni_2P nanolayer on top of Ni_5P_4. Based on quantum mechanical image simulations, a NiP_x ($0 < x < 0.5$) nanolayer was found to reconstruct on surfaces of the Ni_2P-covered Ni_5P_4 matrix, in which the nickel is suggested to be deficient at specific atomic sites. The structure-activity relation exposed here presents a novel insight towards understanding catalytic performance of the nickel phosphides catalysts.

EXPERIMENTAL SECTION

Sample Preparation and Electrochemical Test. The phosphide nanosheets were synthesized by direct phospharization of commercially available Ni foam at 500 °C for 6 h in a tube furnace. X-ray diffraction analysis shows that the Ni_5P_4 and Ni_2P phase takes about 80% and 20% proportion, respectively.[5] As for the TEM specimens, the nanosheets were scrapped down into the ultrapure water using a blade. After dispersing the suspension solution, the copper grid was dried on a plate oven (~ 60 ºC) and then cooled down to room temperature. The HER tests were carried out at room temperature (~25 ºC) in a three-electrode cell in 0.5 M H_2SO_4 solution (pH = 0.28), during which the N_2 bubbling was maintained throughout the experiments. More relevant details are presented elsewhere.[5]

Electron Microscopy Imaging Experiments. Scanning electron microscopy (JEOL, JSM-7400F) was used for sample morphology analysis. An image-corrected FEI Titan 80-300 microscope, with a point resolution better than 80 pm, was operated at 300 kV and used for TEM imaging experiments. An FEI Titan 80-200 Chemi-STEM microscope, equipped with a Super-X energy dispersive X-ray spectrometer and bright-field/dark-field STEM detectors was employed to collect the HAADF images and energy dispersive X-ray spectroscopy (EDX) results. The selected area electron diffraction experiments were performed on an FEI Tecnai F20 microscope. During our electron-beam bombardment experiments, relatively low electron-beam dose rate is used for illuminating thin regions of the phosphide nanosheets.

Image Simulations. The CrystalKit-MacTempas software package was used for TEM image simulations, in which the imaging parameters are determined to be C_S = -10 μm, *A1* = 2.5 nm, *A2* = *B2* = 90 nm, respectively. Dr. Probe[33] software package was used for STEM image simulations.

Being consistent with the experimental conditions, the collection angle range for the HAADF image simulations was set at 70~200 mrad. Meanwhile, different gap distances between the superimposed sublayers were tested to identify their influence to the column intensity, in which a sublayer spacing of ~0.183 nm was used for our HAADF image simulations.

Table 1. List of compositional ratio, precursor, synthesis method, electrolytes and electrocatalytic activity of Ni_5P_4 for the HER. The atomic ratio of Ni/P mainly comes from the EDX analysis.

Morphology Ni/P ratio	Precursors Synthesis method	Electrolytes for HER	Tafel slope ($mVdec^{-1}$)	$\eta_{j=10mAcm^{-2}}$ mV	Ref.
MicroParticle	Nickel, red P	0.5 M H_2SO_4	30	43	[7]
1.19[a]	Solid state reaction	1 M NaOH	121	193	
MicroParticle	Solvothermal	1 M H_2SO_4	33	23	[10]
1.19	Solid state reaction	Base	98	49	
Film	Ni foil, red P	0.5 M H_2SO_4	40	140	[8]
$1.32/1.16_{ICP}$[b]	Contact-conversion	1.0 M KOH	53	150	
NanoCrystal	$Ni(acac)_2$, TOP	0.5 M H_2SO_4	42	118	[31]
1.33	Thermal decomposition				
NanoSheet	Ni foil/foam	0.5 M H_2SO_4	34	114	[32]
1.25[c]	Chemical vapor deposition				
NanoSheet[d]	Ni foam, red P	0.5 M H_2SO_4	53	108	This work
1.45	Vapor solid reaction				

Note: a. The available composition is only from the post-tested Ni_5P_4 MPs.

b. ICP: inductively coupled plasma optical emission spectrometry

c. The ratio measured from the EDX line profiles shown in Fig. 2 therein is Ni/P = 1.34.

d. The Ni_5P_4 phase is coexisting with the Ni_2P phase.

RESULTS AND DISCUSSION

The hexagonal Ni_5P_4, with lattice parameters $a_{54} = b_{54} = 0.6789$ nm and $c_{54} = 1.0989$ nm,[34] is comprised of independent Ni_3P_3, Ni_4P_3 and Ni_3P_2 sublayers (Figure 1a), and the screw 6_3 symmetry leads to their repetition with rotation along the *c* axis. For the hexagonal Ni_2P phase,[21] it is comprised of stacking Ni_3P_1 and Ni_3P_2 sublayers along the *c* axis (Figure 1b). Figure 2a shows morphology of the Ni_5P_4 nanosheets grown on the Ni foam, which are several micrometers in the basal plane. Our statistical observations reveal that the nanosheets are preferentially oriented along the [001] direction (Figure S1). By performing EDX detection, our statistical analysis reveals that Ni is enriched on almost all Ni_5P_4 nanosheets. At the as-grown state, the atomic ratio Ni:P is about 1.45: 1, and this ratio decreases to 1.34: 1 after the HER test in sulfuric acid for 5 hours, which is still higher than the nominal ratio of 1.25: 1 (Figure 2b).

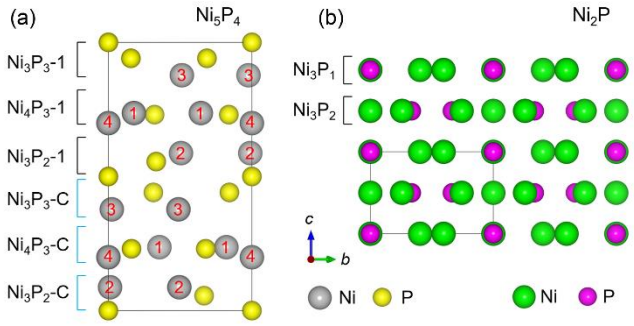

Figure 1. Crystal structure of homogeneous nickel phosphides. (a) [100]-oriented Ni_5P_4 phase (space group $P6_3mc$) with labeling the stacking sequences and Ni atomic sites (Ni1, Ni2, Ni3 and Ni4) within the unit cell. (b) [100]-oriented Ni_2P phase (space group $P\bar{6}2m$) with labeling the stacking sequences along *c* axis.

Figure 2c shows an atomically-resolved TEM image recorded under the negative spherical-aberration imaging (NCSI) conditions.[35-37] By comparing with the simulated image (the inset), we clearly see a sophisticated intensity distribution of atom columns, which is associated with presence of atomic terraces (Figure S2). According to our image simulations, the decreased contrast of collinear Ni/P (cNP) atom columns (blue circles) with increased specimen thickness positions the Ni_5P_4 structural model on the experimental image (Figure S3). Further, the six-fold-symmetric noncollinear Ni/P (ncNP) atom columns (marked by blue hexagons), with strong peak-intensity variation, exhibit prominent reconstruction feature (Figure 2d). This is also hinted by asymmetric intensity feature of <100>* reflection spots in the electron diffraction pattern with respect to the simulated one (Figure S1). For simplicity, positions of the ncNP columns are successively indexed as 0, $\pi/3$, $2\pi/3$, π, $4\pi/3$, $5\pi/3$ point (Figure 2f). Particularly, the $5\pi/3$-point atomic columns (green circles) have the maximum peak intensity. For phosphorous (red circles) atoms bridged by non-collinear Ni2/Ni3 (ncNN) columns, the approximate peak intensities imply that atoms are not obviously reconstructed there.

By means of electron-beam bombardment to the nanosheets, we surprisingly found a thin layer of Ni_2P (~ 3 nm), which is characteristic of three-fold coordination of Ni to P (Figure 2e). Being consistent with the EDX result, this suggests that the surfaces of Ni_5P_4 nanosheets are coated by a thin layer of Ni_2P. Specifically, the observed $\pi/6$ rotation of their primitive unit cells (PUCs) evidences their coherent epitaxy ($a_{21} \approx \sqrt{3}a_{54}/2$) along the [001] direction (Figure 2f). The lattice parameters of Ni_2P phase, a_{21} = 0.5859 nm and c_{21} = 0.3382 nm[38], indicates that the self-epitaxial layer is suffering a compressive strain ~0.3% from the Ni_5P_4 phase. From the overlapped structural models, we clearly see non-collinearity induced elongation of most atom columns and several collinearly aligned columns, e.g., P atoms in Ni_2P with the cNP atoms in Ni_5P_4. For simply

describing their structural relationships, the parallelogram PUCs of both phases are re-shaped into six-fold-symmetric equivalently transformed unit cells (ETUCs) with the identical *c* axes, respectively.

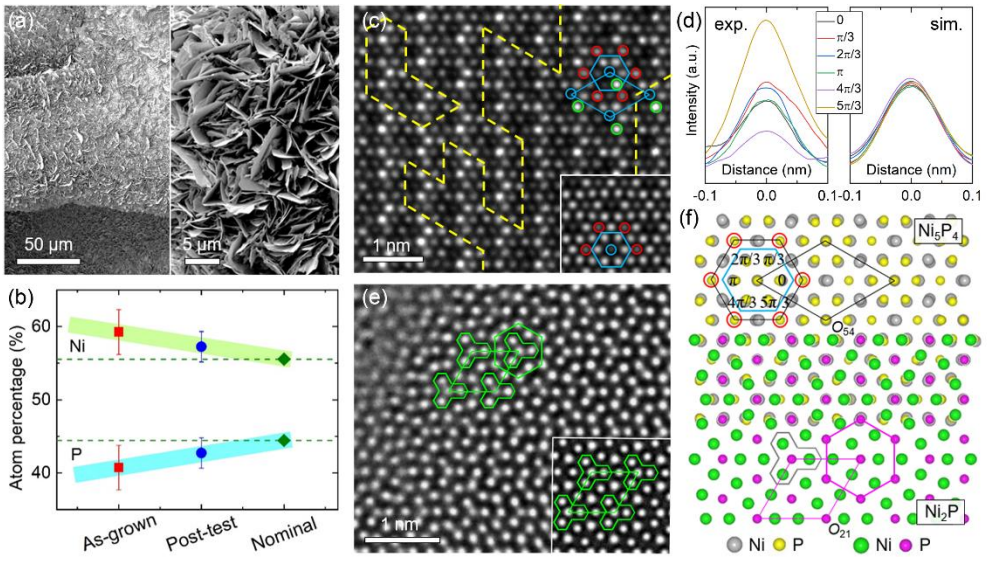

Figure 2. Self-epitaxial growth of Ni_2P layer on surfaces of Ni_5P_4 nanosheet. (a) SEM image of the Ni_xP_y nanosheets and an enlarged view (inset). (b) Composition of as-grown (red), HER-tested (blue) Ni_5P_4 nanosheets compared with the nominal stoichiometry (green). (c) Atomic-resolution TEM image of Ni_5P_4 recorded along the [001] direction and the simulated image (thickness t = 6.2 nm). The yellow dashed lines denote the atomic terraces resulting from surface reconstruction (Figure S2). (d) Intensity profile comparison for the ncNP columns between the experimental and simulated images. (e) Atomic-resolution self-epitaxial Ni_2P phase revealed by electron-beam irradiation on the Ni_5P_4 nanosheet and simulated image (t = 3.0 nm) along the [001] direction. (f) Lattice match relation between Ni_5P_4 and Ni_2P along their common [001] direction. The PUC and ETUC of Ni_5P_4 and Ni_2P phases are denoted by black and pink polygons, respectively.

It is noteworthy that the reconstruction feature is also observed in our high-angle annular-dark-field (HAADF) STEM images of the HER-tested nanosheets, where the brightest ncNP atom columns within the blue hexagons appear at the 0-point positions (Figure 3a). A large-area image showing a uniform surface reconstruction of atoms is presented in Figure S4. Since the image contrast of HAADF image is proportional to $\sim Z^2$ (Z = atomic number),[39] the atoms with smaller Z, e.g., P (Z = 15), O (Z = 8) and H (Z = 1), on surface of the Ni_5P_4 phase are therefore invisible owing to their weak scattering ability to the incident electrons. Being consistent with the simulated image (inset in Figure 3a), this clearly signifies reconstruction of heavy Ni (Z = 28) atoms on top of these P-occupying positions (red circles), which does not exclude the presence of surface species like H_2O and PH_x. With respect to the experimental image, we also noted absence of elongated ncNP atom columns in the simulated image. Furthermore, we see that the ncNN atom columns always have the strongest peak intensities.

Since the HAADF-STEM images mainly collect signals from the heavy Ni atoms, the surface structure disclosed by this method, to a certain degree, decomposes the reconstruction feature manifested by the TEM results. For simplicity, the atomic surface reconstruction is hereafter deciphered through simulation-based measurement of the HAADF images. Referring to the peak intensity of the cNP columns (marked by blue circles), all column-peak intensities are measured and plotted in polar coordinates. Within the blue hexagons (Figure 3b), the $\pi/3$- and $5\pi/3$-point columns have the lowest intensity, identical to the reference cNP column (blue circle), and the $2\pi/3$-, π-, $4\pi/3$-point columns have an intermediate intensity. Within the neighboring green hexagon (Figure 3a,c), the 0-point ncNN columns and all ncNP columns have stronger peak intensity than the reference column. Meanwhile, the 0-point ncNP column also has stronger peak intensity than the $2\pi/3$- and $4\pi/3$-point columns within the orange hexagon (Figure 3d). In addition,

the collinear P columns (yellow atoms and denoted by red circles) in the green and orange hexagons also have different peak intensities. In fact, the HAADF-STEM images also unveil a complex reconstruction feature of atoms on the phosphide surface.

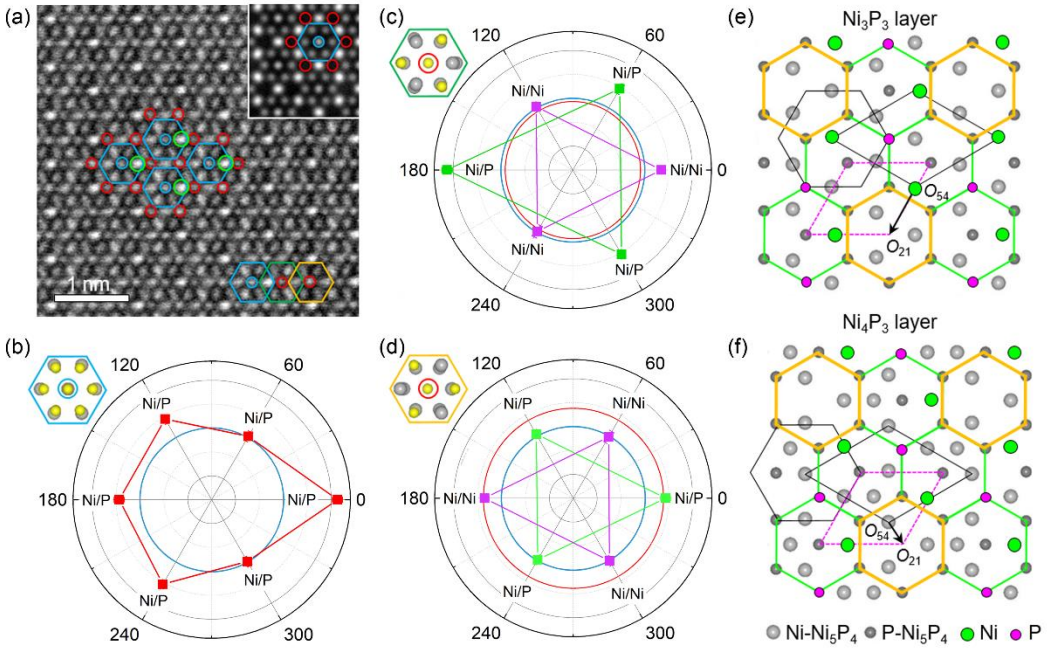

Figure 3. Termination dependent reconstruction of Ni_2P on top of Ni_5P_4. (a) Atomic-resolution HAADF-STEM image of Ni_5P_4 collected along [001] direction and a simulated image (thickness t = 40 nm). (b-d) Polar-coordinate plots of peak intensity (radial direction), normalized by intensity of the cNP columns, measured from atom columns within the blue, green and yellow hexagons illustrated in (a). (e,f) Analysis of reconstructed Ni_2P (colorful PUC and ETUC) on Ni_3P_3-terminated and Ni_4P_3-terminated Ni_5P_4 (black PUC and ETUC). The green and pink circles denote the possibly reconstructed Ni and P atoms and the black arrows mark the unit-cell shift of the two structural phases.

To find out origin of the surface reconstruction, the sublayer structural features of Ni_5P_4 are analyzed along the [001] direction. Given their lattice match relationship, the (001)-oriented sublayers of Ni_5P_4 are re-partitioned by the ETUCs of Ni_2P. It is surprisingly found that the Ni_3P_3 sublayer is comprised of two kinds of $ETUCs_{21}$ (Figure 3e), periodic Ni_3P_2 (orange hexagons) gapped by interconnected $Ni_2P_{7/3}$ (green hexagons). Obviously, the Ni_3P_2 hexagons provide a favorable condition for epitaxial growth of Ni_2P on top of Ni_5P_4, and additional filling of Ni (green circles) and P (pink circles) atoms at certain positions may possibly happen at the (001) interface of the two phases. Analogously, the Ni_4P_3 sublayer, comprising of Ni_3P_2 (orange) and $Ni_3P_{7/3}$ (green) $ETUC_{21}$, may also be favorable for the epitaxial growth (Figure 3f). Nevertheless, the Ni_3P_2 sublayer does not show features of facilitating construction of Ni_2P on top of Ni_5P_4 (Figure S5).

On this basis, the atomic reconstructions on Ni_5P_4 (001) surfaces were examined by image simulations, in which the Ni_4P_3-terminated Ni_5P_4 was superimposed by a layer of Ni_2P (Figure 4a). At positions of pure P-occupying positions, despite overlaying of Ni atoms in Ni_2P on the top, clear column intensities can hardly be discerned from the simulated image. Only when an additional layer of Ni atoms is superimposed on top of Ni_2P, the prominent reconstruction features can be reproduced, e.g., the column intensities at pure P-occupying positions and the 0-point ncNP within the blue hexagons (Figure 4b). Judging from the intensity profiles of the ncNP columns, our simulation suggests that thickness of the top-most Ni layer is about 2 nm (Figure 4c,d). It should be noted that the electron channeling effects[40] also lead to intensity variation of neighboring non-reconstructed columns. Meanwhile, the P atoms may also be involved in the surface atom reconstruction.

A schematic structure model corresponding to the simulated image is presented along the plan-view direction (Figure 4e). It can be seen that the reconstructed Ni atoms do not alter

periodicity of the Ni_5P_4 lattices. Therefore, the surface atom reconstruction is not manifested by presence of superstructure spots in the electron diffraction patterns (Figure S1). In addition, we found that the nickel atoms at specific sites (Ni2, Ni3 and Ni4) of Ni_5P_4 tend to be deficient (Figure 1a). This is evidenced by a dramatic intensity mismatch of the ncNN columns between the experimental and the simulated images of Ni_5P_4 at an ideal stoichiometry (Figure 3a and inset). Without considering the nickel deficiencies, the ncNN columns always have the strongest intensities, leading to failure in reproducing the experimentally observed reconstruction features, even with overlapping of Ni_2P on the top (Figure S6). According to our image simulations, it is estimated that the occupation (Occ.) of nickel is $Occ._{Ni2} = Occ._{Ni3} = 0.6$ and $Occ._{Ni4} = 0.8$ (Figure 4c). The structural parameters used for the image simulations are presented in Table S1.

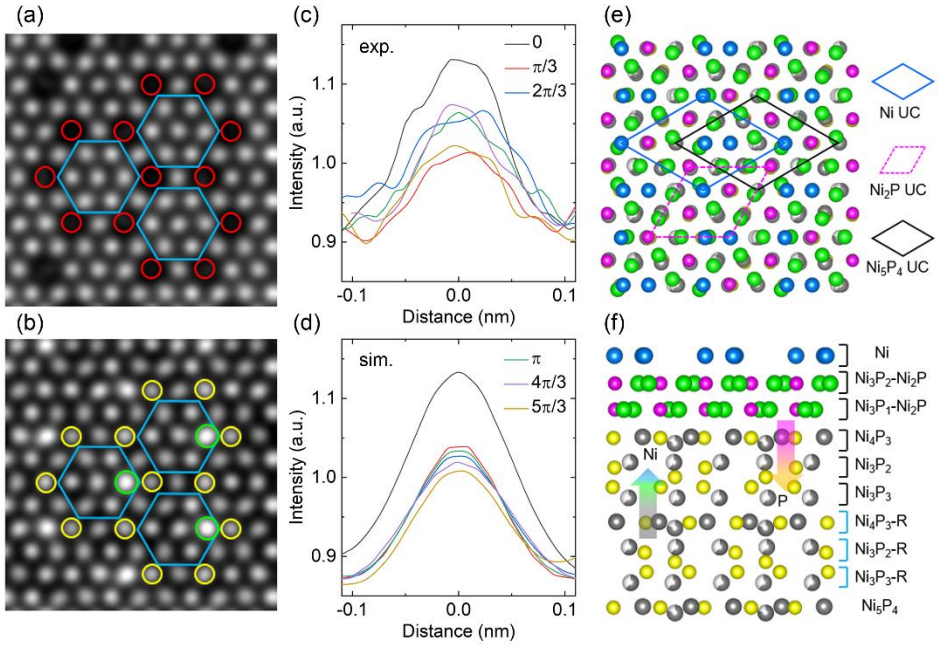

Figure 4. Surface chemical gradients unveiled by quantitative image simulations. (a) Simulated HAADF image of Ni_2P (2.2nm)/Ni_5P_4 (38.5nm) bilayer along the [001] direction. (b) Simulated image of Ni (1.9nm)/Ni_2P (2.2nm)/Ni_5P_4 (38.5nm) triple-layer structure. The green and yellow circles denote the reconstructed Ni atoms at 0-point positions within the blue hexagons and

at positions of pure P atoms in Ni_5P_4. (c,d) Intensity profiles of ncNP columns within the blue hexagons from the experimental and simulated image, respectively. (e) Schematic plan view of the $Ni/Ni_2P/Ni_5P_4$ layered structure along the $[001]_{54}$ direction. (f) Schematic cross-section view of the $Ni/Ni_2P/Ni_5P_4$ layered structure along the $[010]_{54}$ direction. The arrows denote the diffusion direction of Ni and P in the multi-layer structure.

With respect to the self-epitaxial hetero-nanolayers, the cationic vacancies identified in the Ni_5P_4 phase reveal that the Ni atoms possess high thermodynamic activity. That is to say, under non-equilibrium thermal conditions, i.e., during the phosphorization process,[5] the Ni atoms diffuse quickly towards the exterior surfaces associated with an inverse diffusion of P atoms towards the interior (Figure 4f). This explains why the Ni tends to be enriched on surfaces of the phosphides. It should be noted that the surface Ni atoms are not existing in an elemental form. Its valence in the range of 0 ~ 1, as detected by X-ray photoelectron spectroscopy (XPS) (Figure S7), shows that the Ni atoms may reconstruct together with the P atoms, which probably form a layer of NiP_x ($0 < x < 0.5$) on the phosphide surfaces. Such a hetero-epitaxial scenario is further supported by complex reconstruction of NiP_x on surfaces of the Ni_2P nanosheets (Figure S8), which yields an atomic ratio of $Ni/P = 2.16 \pm 0.25$.

Regarding proportion of the Ni_2P phase in the Ni_xP_y nanosheets, our previous quantitative X-ray diffraction analysis reveals that it takes about 22% in the as-grown sample,[5] which decreases to ~18% after 72 h HER test in N_2-saturated 0.5 M H_2SO_4 electrolyte. According to our statistical observations, nevertheless, only a few (less than 5) Ni_2P-dominant nanosheets were identified among tens of them (~50). This suggests that most of the Ni_2P phase undergoes an epitaxial growth on surfaces of the Ni_5P_4 phase. Assuming the Ni_2P: Ni_5P_4 phase ratio is 1:4, for a nanosheet with

a thickness of 10 or 100 nm, thickness of the self-epitaxial Ni_2P phase is 2 or 20 nm, being consistent with our result presented in Figure 2e. The polarization curves with the *iR* correction (i.e., electrolyte resistance compensation) for the heterogeneous nanosheets are measured and presented (Figure 5a). Compared with the 15% Pt/C catalyst, we see that an overpotential (η) value of η = 108, 147 and 169 mV is required to achieve a current density (j) of 10, 50 and 100 mA cm^{-2} for the as-grown nanosheets. After two accelerated degradation tests (ADTs), the overpotential individually increases to 117, 158 and 183 mV to achieve the same current densities. Correspondingly, a linear fitting to the η vs log (j) relation reveals that the Tafel slope increases from 53.1 to 56.2 mV dev^{-1}, which is 38.2 mV dev^{-1} for the Pt/C catalyst (Figure 5b).

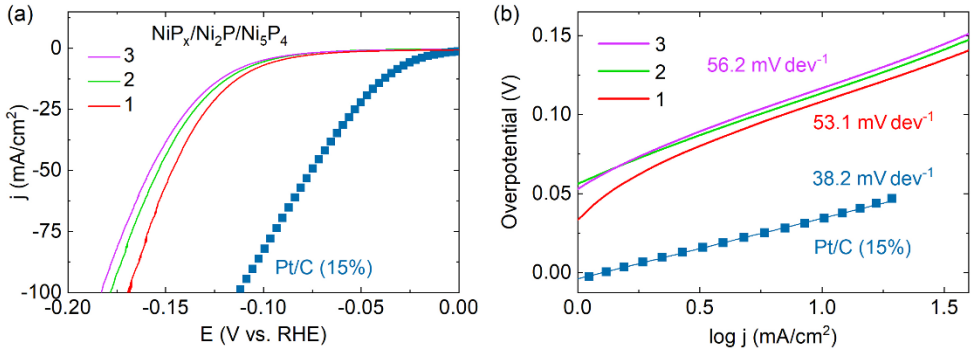

Figure 5. Catalytic performance of the heterostructure nanosheets in N_2-saturated 0.5 M H_2SO_4. (a) Polarization (LSV) curves and (b) Tafel plots measured before and after each 1000-cycle ADT with respect to the commercial Pt/C (15%) catalyst. The scan rate is 5 mV s^{-1}.

Regarding presence of the self-epitaxial hetero-nanolayers, this can be ascribed to the following reasons. Firstly, since the nanosheets were formed by vapor phosphorization to the Ni foam, the obvious chemical gradients during the synthesis are not favorable for formation of single-phase nickel phosphides,[6, 41] which are sensitive to the Ni-P atomic ratio of the precursors.[31]

Secondly, given the coherent (001) planes of the sublayers of both phases, the high thermodynamic activity of nickel favors the self-epitaxy of Ni_2P on top of the Ni_5P_4 phase. Thirdly, the formation temperature of the Ni_2P phase is lower than that of the Ni_5P_4 phase,[5, 41] which also provides a favorable condition for epitaxial growth of the former phase on top of the latter phase during the cooling procedure of sample preparation. Therefore, with respect to the composition-activity relation summarized in Table 1, particularly the P-rich Ni_5P_4, our results suggest that the passivated catalytic activity is possibly attributed to the surface reconstruction arising from the Ni enrichment. This also provides a reference for understanding the catalytic activity of other Ni-containing catalysts, e.g., Ni_3P, $Ni_{12}P_5$, Ni_3S_2 and NiSe.[7, 42-44]

CONCLUSION

Our atomic-scale structural study reveals a self-epitaxial growth of Ni_2P and NiP_x ($0 < x < 0.5$) nanolayers on top of (001)-oriented Ni_5P_4 phase, which should passivate the intrinsic catalytic activity of the Ni_5P_4 phase. Besides the structural driving force arising from similarity of their sublayers, the self-epitaxy of heterogeneous nanolayers may also be influenced by the synthesis method, precursor, temperature factor and so on. Particularly, the identified surface chemical gradient associated with the core-shell configuration, driven by the high thermodynamic activity of nickel, innovates our traditional understanding on surface microstructures of the nickel phosphides. Therefore, it is believed that the findings offer a new perspective to understand performance of the transition-metal catalysts, e.g., phosphides, sulfides and selenides. It also highlights the importance of performing atomic-scale 3D characterization to better configure the structure-activity relationship in electrochemical energy conversion.

ASSOCIATED CONTENT

Supporting Information

Morphology and selected area electron diffraction of the Ni_5P_4 nanosheet (Figure S1); atomic-terraces identified from the atomic-resolution TEM image (Figure S2); identification of the atom column positions by means of image simulation (Figure S3); large-field view of the atomic-scale surface reconstruction from the HAADF-STEM image (Figure S4); repartition of Ni_3P_2 sublayer of the Ni_5P_4 phase by the ETUCs of Ni_2P (Figure S5); simulated HAADF-STEM images of the [001]-oriented Ni_5P_4 phase with consideration of different Ni vacancies and overlapping of Ni_2P directly on Ni_5P_4 (Figure S6); XPS spectra of Ni $2p_{3/2}$ before and after the HER test (Figure S7) and enrichment of Ni identified from [001]-oriented Ni_2P phase (Figure S8).

AUTHOR INFORMATION

Corresponding Author

Xian-Kui Wei - Ernst Ruska-Centre for Microscopy and Spectroscopy with Electrons, Forschungszentrum Jülich GmbH, Jülich 52428, Germany; orcid.org/0000-0003-4320-1120; Email: x.wei@fz-juelich.de

Authors

Dehua Xiong - State Key Laboratory of Silicate Materials for Architectures, Wuhan University of Technology, Wuhan 430070, China; orcid.org/0000-0002-4714-9019

Lifeng Liu - International Iberian Nanotechnology Laboratory (INL), Braga 4715-330, Portugal; orcid.org/0000-0002-0187-9243

Rafal E. Dunin-Borkowski - Ernst Ruska-Centre for Microscopy and Spectroscopy with Electrons, Forschungszentrum Jülich GmbH, Jülich 52428, Germany; orcid.org/0000-0001-8082-0647

Notes

The authors declare no competing financial interests

ACKNOWLEDGEMENTS

This work is supported by the European Union's Horizon 2020 research and innovation program through the CritCat Project under grant agreement No. 686053.

References

(1) Li, Y.; Dong, Z.; Jiao, L., Multifunctional transition metal-based phosphides in energy-related electrocatalysis. *Adv. Energy Mater.* **2019**, *10*, 1902104.

(2) Zou, X.; Zhang, Y., Noble metal-free hydrogen evolution catalysts for water splitting. *Chem. Soc. Rev.* **2015,** *44*, 5148-5180.

(3) Wang, Y.; Kong, B.; Zhao, D.; Wang, H.; Selomulya, C., Strategies for developing transition metal phosphides as heterogeneous electrocatalysts for water splitting. *Nano Today* **2017,** *15*, 26-55.

(4) Xiao, P.; Sk, M. A.; Thia, L.; Ge, X.; Lim, R. J.; Wang, J.-Y.; Lim, K. H.; Wang, X., Molybdenum phosphide as an efficient electrocatalyst for the hydrogen evolution reaction. *Energy Environ. Sci.* **2014,** *7*, 2624-2629.

(5) Wang, X. G.; Kolen'ko, Y. V.; Bao, X. Q.; Kovnir, K.; Liu, L. F., One-step synthesis of self-supported nickel phosphide nanosheet array cathodes for efficient electrocatalytic hydrogen generation. *Angew. Chem. Int. Edit.* **2015,** *54*, 8188-8192.

(6) Wang, X.; Li, W.; Xiong, D.; Petrovykh, D. Y.; Liu, L., Bifunctional nickel phosphide nanocatalysts supported on carbon fiber paper for highly efficient and stable overall water splitting. *Adv. Funct. Mater.* **2016,** *26*, 4067-4077.

(7) Laursen, A. B.; Wexler, R. B.; Whitaker, M. J.; Izett, E. J.; Calvinho, K. U. D.; Hwang, S.; Rucker, R.; Wang, H.; Li, J.; Garfunkel, E.; Greenblatt, M.; Rappe, A. M.; Dismukes, G. C., Climbing the volcano of electrocatalytic activity while avoiding catalyst corrosion: Ni_3P, a hydrogen evolution electrocatalyst stable in both acid and alkali. *ACS Catal.* **2018,** *8*, 4408-4419.

(8) Ledendecker, M.; Calderon, S. K.; Papp, C.; Steinruck, H. P.; Antonietti, M.; Shalom, M., The synthesis of nanostructured Ni_5P_4 films and their use as a non-noble bifunctional electrocatalyst for full water splitting. *Angew. Chem. Int. Edit.* **2015,** *54*, 12361-12365.

(9) Popczun, E. J.; McKone, J. R.; Read, C. G.; Biacchi, A. J.; Wiltrout, A. M.; Lewis, N. S.; Schaak, R. E., Nanostructured nickel phosphide as an electrocatalyst for the hydrogen evolution reaction. *J. Am. Ceram. Soc.* **2013,** *135*, 9267-9270.

(10) Laursen, A. B.; Patraju, K. R.; Whitaker, M. J.; Retuerto, M.; Sarkar, T.; Yao, N.; Ramanujachary, K. V.; Greenblatt, M.; Dismukes, G. C., Nanocrystalline Ni_5P_4: a hydrogen evolution electrocatalyst of exceptional efficiency in both alkaline and acidic media. *Energy Environ. Sci.* **2015,** *8*, 1027-1034.

(11) Stern, L. A.; Feng, L. G.; Song, F.; Hu, X. L., Ni_2P as a Janus catalyst for water splitting: the oxygen evolution activity of Ni_2P nanoparticles. *Energy Environ. Sci.* **2015,** *8*, 2347-2351.

(12) Xu, J.; Wei, X.-K.; Costa, J. D.; Lado, J. L.; Owens-Baird, B.; Gonçalves, L. P. L.; Fernandes, S. P. S.; Heggen, M.; Petrovykh, D. Y.; Dunin-Borkowski, R. E.; Kovnir, K.; Kolen'ko, Y. V., Interface engineering in nanostructured nickel phosphide catalyst for efficient and stable water oxidation. *ACS Catal.* **2017,** *7*, 5450-5455.

(13) Oyama, S. T., Novel catalysts for advanced hydroprocessing: transition metal phosphides. *J. Catal.* **2003,** *216*, 343-352.

(14) Calvinho, K. U. D.; Laursen, A. B.; Yap, K. M. K.; Goetjen, T. A.; Hwang, S.; Murali, N.; Mejia-Sosa, B.; Lubarski, A.; Teeluck, K. M.; Hall, E. S.; Garfunkel, E.; Greenblatt, M.; Dismukes, G. C., Selective CO_2 reduction to C3 and C4 oxyhydrocarbons on nickel phosphides at overpotentials as low as 10 mV. *Energy Environ. Sci.* **2018,** *11*, 2550-2559.

(15) Hernandez, A. B.; Ariga, H.; Takakusagi, S.; Kinoshita, K.; Suzuki, S.; Otani, S.; Oyama, S. T.; Asakura, K., Dynamical LEED analysis of Ni_2P (0001)-1×1: Evidence for P-covered surface structure. *Chem. Phys. Lett.* **2011,** *513*, 48-52.

(16) Wang, Z.; Heng, N.; Wang, X.; He, J.; Zhao, Y., Surface and morphology structure evolution of metal phosphide for designing overall water splitting electrocatalyst. *J. Catal.* **2019**, *374*, 51-59.

(17) Wexler, R. B.; Martirez, J. M. P.; Rappe, A. M., Stable phosphorus-enriched (0001) surfaces of nickel phosphides. *Chem. Mater.* **2016,** *28*, 5365-5372.

(18) Wexler, R. B.; Martirez, J. M. P.; Rappe, A. M., Active role of phosphorus in the hydrogen evolving activity of nickel phosphide (0001) surfaces. *ACS Catal.* **2017,** *7*, 7718-7725.

(19) Wexler, R. B.; Martirez, J. M. P.; Rappe, A. M., Chemical pressure-driven enhancement of the hydrogen evolving activity of Ni_2P from nonmetal surface doping interpreted via machine learning. *J. Am. Chem. Soc.* **2018,** *140*, 4678-4683.

(20) Liu, P.; Rodriguez, J. A., Catalysts for hydrogen evolution from the [NiFe] hydrogenase to the Ni_2P (001) surface: The importance of ensemble effect. *J. Am. Ceram. Soc.* **2005,** *127,* 14871-14878.

(21) Li, Q.; Hu, X., First-principles study of Ni_2P (0001) surfaces. *Phys. Rev. B* **2006,** *74*, 035414.

(22) Li, H.; Tsai, C.; Koh, A. L.; Cai, L.; Contryman, A. W.; Fragapane, A. H.; Zhao, J.; Han, H. S.; Manoharan, H. C.; Abild-Pedersen, F.; Norskov, J. K.; Zheng, X., Activating and optimizing MoS_2 basal planes for hydrogen evolution through the formation of strained sulphur vacancies. *Nat. Mater.* **2016,** *15*, 364.

(23) Ye, G.; Gong, Y.; Lin, J.; Li, B.; He, Y.; Pantelides, S. T.; Zhou, W.; Vajtai, R.; Ajayan, P. M., Defects engineered monolayer MoS_2 for improved hydrogen evolution reaction. *Nano Lett.* **2016,** *16*, 1097-1103.

(24) Kibsgaard, J.; Chen, Z.; Reinecke, B. N.; Jaramillo, T. F., Engineering the surface structure of MoS_2 to preferentially expose active edge sites for electrocatalysis. *Nat. Mater.* **2012,** *11*, 963-969.

(25) Kibsgaard, J.; Jaramillo, T. F., Molybdenum phosphosulfide: an active, acid-stable, earth-abundant catalyst for the hydrogen evolution reaction. *Angew. Chem. Int. Edit.* **2014,** *53*, 14433-14437.

(26) Chang, J.; Li, K.; Wu, Z.; Ge, J.; Liu, C.; Xing, W., Sulfur-doped nickel phosphide nanoplates arrays: a monolithic electrocatalyst for efficient hydrogen evolution reactions. *ACS Appl. Mater. Interfaces* **2018,** *10*, 26303-26311.

(27) Liu, K.; Wang, F.; He, P.; Shifa, T. A.; Wang, Z.; Cheng, Z.; Zhan, X.; He, J., The role of active oxide species for electrochemical water oxidation on the surface of 3*d*-metal phosphides. *Adv. Energy Mater.* **2018,** *8*, 1703290.

(28) Li, Z.; Dou, X.; Zhao, Y.; Wu, C., Enhanced oxygen evolution reaction of metallic nickel phosphide nanosheets by surface modification. *Inorg. Chem. Front.* **2016,** *3*, 1021-1027.

(29) Rundqvist, S., X-ray investigations of Mn_3P, Mn_2P and Ni_2P. *Acta Chem. Scandi.* **1962,** *16*, 992.

(29) Hansen, M. H.; Stern, L. A.; Feng, L.; Rossmeisl, J.; Hu, X., Widely available active sites on Ni_2P for electrochemical hydrogen evolution--insights from first principles calculations. *Phys. Chem. Chem. Phys.* **2015,** *17*, 10823-10829.

(30) Kibsgaard, J.; Tsai, C.; Chan, K.; Benck, J. D.; Nørskov, J. K.; Abild-Pedersen, F.; Jaramillo, T. F., Designing an improved transition metal phosphide catalyst for hydrogen evolution using experimental and theoretical trends. *Energy & Environ. Sci.* **2015,** *8*, 3022-3029.

(31) Pan, Y.; Liu, Y.; Zhao, J.; Yang, K.; Liang, J.; Liu, D.; Hu, W.; Liu, D.; Liu, Y.; Liu, C., Monodispersed nickel phosphide nanocrystals with different phases: synthesis, characterization and electrocatalytic properties for hydrogen evolution. *J. Mater. Chem. A* **2015,** *3*, 1656-1665.

(32) Jung, C. S.; Park, K.; Lee, Y.; Kwak, I. H.; Kwon, I. S.; Kim, J.; Seo, J.; Ahn, J.-P.; Park, J., Nickel phosphide polymorphs with an active (001) surface as excellent catalysts for water splitting. *CrystEngComm* **2019,** *21*, 1143-1149.

(33) Barthel, J., Dr. Probe: A software for high-resolution STEM image simulation. *Ultramicroscopy* **2018,** *193*, 1-11.

(34) Babizhetskyy, V.; Kotur, B.; Oryshchyn, S.; Zheng, C.; Kneidinger, F.; Leber, L.; Simson, C.; Bauer, E.; Michor, H., Crystal and electronic structure and physical properties of Ni_5P_4. *Solid State Commun.* **2013,** *164*, 1-5.

(35) Jia, C. L.; Lentzen, M.; Urban, K., Atomic-resolution imaging of oxygen in perovskite ceramics. *Science* **2003,** *299*, 870-873.

(36) Wei, X.-K.; Yang, Y.; McGilly, L. J.; Feigl, L.; Dunin-Borkowski, R. E.; Jia, C.-L.; Bellaiche, L.; Setter, N., Flexible polarization rotation at the ferroelectric/metal interface as a seed for domain nucleation. *Phys. Rev. B* **2018,** *98*, 020102(R).

(37) Wei, X. K.; Jia, C. L.; Du, H. C.; Roleder, K.; Mayer, J.; Dunin-Borkowski, R. E., An unconventional transient phase with cycloidal order of polarization in energy-storage antiferroelectric $PbZrO_3$. *Adv Mater* **2020,** 32, 1907208.

(38) Rundqvist, S., X-ray investigations of Mn_3P, Mn_2P and Ni_2P. *Acta Chem. Scandi.* **1962,** *16*, 992.

(39) Nellist, P. D.; Pennycook, S. J., The principles and interpretation of annular dark-field Z-contrast imaging. *Adv. Imag. Elect. Phys.* **2000,** *113*, 147-203.

(40) Haruta, M.; Kurata, H.; Komatsu, H.; Shimakawa, Y.; Isoda, S., Effects of electron channeling in HAADF-STEM intensity in La_2CuSnO_6. *Ultramicroscopy* **2009,** *109*, 361-367.

(41) Li, J.; Zhou, X.; Xia, Z.; Gao, W.; Ma, Y.; Qu, Y., Highly efficient and robust nickel phosphides as bifunctional electrocatalysts for overall water-splitting. *ACS Appl. Mater. Interfaces* **2016,** *8*, 10826.

(42) Huang, Z.; Chen, Z.; Chen, Z.; Lv, C.; Meng, H.; Chi Zhang, $Ni_{12}P_5$ Nanoparticles as an efficient catalyst for hydrogen generation via electrolysis and photoelectrolysis. *ACS Nano* **2014,** *8*, 8121-8129.

(43) Yang, C.; Gao, M. Y.; Zhang, Q. B.; Zeng, J. R.; Li, X. T.; Abbott, A. P., In-situ activation of self-supported 3D hierarchically porous Ni_3S_2 films grown on nanoporous copper as excellent pH-universal electrocatalysts for hydrogen evolution reaction. *Nano Energy* **2017,** *36*, 85-94.

(44) Zou, Z.; Wang, X.; Huang, J.; Wu, Z.; Gao, F., An Fe-doped nickel selenide nanorod/nanosheet hierarchical array for efficient overall water splitting. *J. Mater. Chem. A* **2019,** *7*, 2233-2241.

1 Table Of Contents (TOC)

Surface atom reconstruction: NiP_x/Ni_2P nanolayers on Ni_5P_4

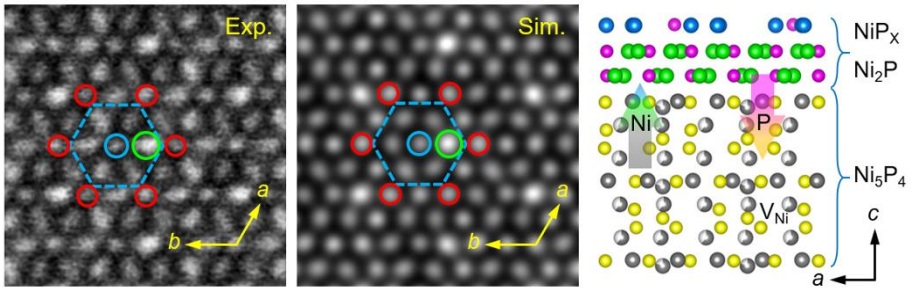

2